J. Fluid Mech. (1985), *vol.* 160, *pp.* 369–383
Printed in Great Britain

The flow of a viscous incompressible fluid past a normal flat plate at low and intermediate Reynolds numbers: the wake

By J. D. HUDSON
Department of Applied and Computational Mathematics, University of Sheffield, England

AND S. C. R. DENNIS
Department of Applied Mathematics, University of Western Ontario, London, Ontario, Canada

(Received 14 May 1984 and in revised form 2 January 1985)

The Navier–Stokes equations are solved numerically for the steady separated flow past a normal flat plate for Reynolds numbers in the range $0.1 \leqslant R \leqslant 20$. Eddy dimensions together with the position of the vortex centre are presented and compared with the few other estimates and predictions available. Streamlines and equivorticity lines are also given. The main result of interest is the extremely good comparison with experimental results over this range of Reynolds numbers. The method of solution is based on an artificial time-dependent procedure using a distorted time. Results are given only for the steady-state flow.

1. Introduction

The primary objective of the present investigation is to obtain numerical solutions of the Navier–Stokes equations for the steady laminar flow of a viscous incompressible fluid past a normal flat plate. Although there has been considerable interest for many years in steady separated flows past various bluff bodies, very little has been reported to date on the special case of the normal flat plate. Of those authors who have considered the theoretical aspects of this problem, most have restricted their attention to the Oseen linearized equations. For example, using these simplified equations, Tomotika & Aoi (1953), Tameda & Miyagi (1962) and Miyagi (1968) have obtained estimates of the drag coefficient; Imai (1957) and Miyagi (1978) have predicted the critical Reynolds number at which separation first occurs, while the latter has additionally estimated the length of the standing vortex pair at low Reynolds numbers. The vortex size has also been estimated by Smith (1979) from asymptotic theory. Published experimental results on the problem are equally sparse. Batchelor (1967) has reproduced some results of Prandtl & Tietjens (1934) while more recent work has been carried out by Acrivos *et al.* (1968) and Taneda (1968).

While there is some agreement between the theoretical and experimental results, the two approaches are not entirely consistent in their conclusions. For example, both Imai (1957) and Miyagi (1978) predict that there exists a vortex pair of vanishing thickness at vanishing Reynolds number, but point out that this is in conflict with the experimental work of Taneda (1968), whose results suggest that separation occurs at $R = 0.4$. Similarly, for higher Reynolds numbers, Acrivos *et al.* (1968) claim that their experimental results support an earlier theoretical model of Acrivos *et al.* (1965) in which the width of the closed wake attains a limit $O(1)$ with increasing Reynolds

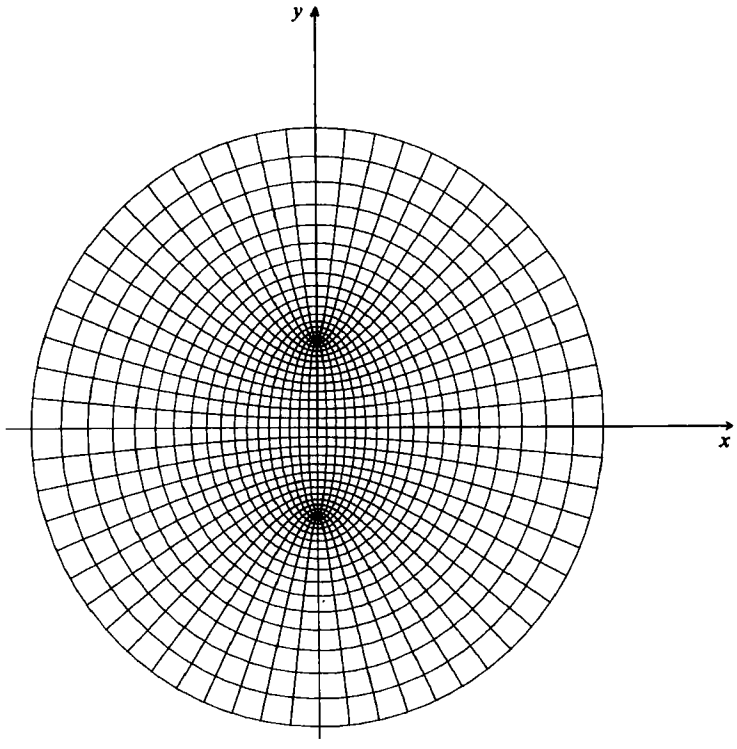

FIGURE 1. The finite-difference grid.

number. However, this is disputed by Smith (1979), who obtains the limit $O(R^{\frac{1}{2}})$ and suggests that the findings of Acrivos *et al.* (1968) are contaminated by the effects of the confining walls. It is therefore hoped that the present finite-difference solutions of the full Navier–Stokes equations will provide additional information which will help in our understanding of this problem, at least for low and intermediate Reynolds numbers.

One of the main difficulties – and a possible source of substantial error – associated with the numerical solution of the Navier–Stokes equations, for flow past any bluff body, is in the determination of the boundary conditions at the common solid/fluid interface. This has been discussed by several authors, including Hudson (1974) and Dennis & Hudson (1980), and applies whether the problem is formulated in terms of the stream function and vorticity distribution, or in terms of the primitive variables. In either case, only the velocity components at the common interface are known from the physics of the problem, the other variables having to be approximated by some means or other. As this is likely to be particularly difficult for the normal flat plate, especially near the edges of the plate, it would be extremely useful to have a method of solution that does not require knowledge of either the pressure or the vorticity on the solid/fluid interface. Fortunately such a method has been devised by Belotserkovskii, Gushchin & Shchennikov (1975) and involves the splitting of the time-dependent equations of motion as proposed by Harlow & Welch (1965). However, unlike the MAC method and its modifications, the finite-difference scheme of Belotserkovskii *et al.* requires only a knowledge of the velocity components on the solid surface: a modified form of this method is therefore used as the basis of the present computations.

Hence the problem was formulated in terms of the pressure p and the velocity components (u, v), and the time-dependent forms of these equations were solved until the steady-state solution was attained. However, as described later, it proved necessary to introduce an element of time distortion into these equations in order to preserve numerical stability, so the intermediate solutions of the time-dependent equations have no physical significance. As the flow is expected to vary most rapidly near to the edges of the plate the graded mesh of figure 1 was employed for the finite-difference approximations.

Reynolds numbers in the range $0.1 \leqslant R \leqslant 20$ were considered. In most cases converged solutions were obtained for different positions of the outer boundary, this being placed at successively increasing distances from the plate and its effect on the solution in the neighbourhood of the plate examined. Furthermore, a very strict exit tolerance was imposed on the iterative procedures in order to prevent premature termination of the calculations.

In this paper the results of the computations are presented in the form of streamlines and equivorticity lines, together with wake dimensions and the positions of the vortex centre, all at various Reynolds numbers up to 20. Some computational details are also given. The range of Reynolds numbers has been restricted to that over which there is reasonable certainty that the properties presented are accurate. No elaborate treatment of the boundary conditions at large distances from the plate is given, but the tests that have been carried out on the positioning of the outer boundary provide satisfactory accuracy checks. The treatment of flow normal to a flat plate by numerical methods is by no means simple owing to the presence of singularities in the vorticity and pressure at the edges. The method used here avoids the difficulties associated with these singularities.

2. Basic equations

With respect to rectangular Cartesian coordinates, the equations governing the flow may be written

$$\frac{\partial u}{\partial t}+\frac{\partial u^2}{\partial x}+\frac{\partial (uv)}{\partial y}=-\frac{1}{\rho}\frac{\partial p}{\partial x}+\nu\left[-\frac{\partial^2 v}{\partial x\,\partial y}+\frac{\partial^2 u}{\partial y^2}\right], \tag{1}$$

$$\frac{\partial v}{\partial t}+\frac{\partial (uv)}{\partial x}+\frac{\partial v^2}{\partial y}=-\frac{1}{\rho}\frac{\partial p}{\partial y}+\nu\left[\frac{\partial^2 v}{\partial x^2}-\frac{\partial^2 u}{\partial x\,\partial y}\right], \tag{2}$$

$$\frac{\partial u}{\partial x}+\frac{\partial v}{\partial y}=0, \tag{3}$$

where (u, v) are the velocity components, p the pressure, ρ the density and ν the coefficient of kinematic viscosity. Equations (1) and (2) are written in conservation form. This is the basic form considered by Belotserkovskii *et al.* (1975), and their method has been adapted directly to the present case, where elliptic coordinates are appropriate. We could equally formulate the equations appropriate to the non-conservation form corresponding to (1) and (2). The plate of length $2l$ is placed coincident with the y-axis with its centre at the origin and, at large distance, the fluid is assumed to be flowing with velocity U parallel to the x-axis. The problem is thus symmetrical about the x-axis, so only the upper half of the (x, y)-plane need be considered. Boundary conditions for u and v are then

$$\left.\begin{aligned} u = v = 0 \quad &\text{on} \quad x = 0, \quad 0 \leqslant y \leqslant l, \\ u \to U, \quad v \to 0 \quad &\text{as} \quad x, y \to \infty. \end{aligned}\right\} \tag{4}$$

It is convenient to make the transformation

$$x = l \sinh \xi \cos \eta, \quad y = l \cosh \xi \sin \eta \tag{5}$$

so that the upper half of the (x, y)-plane is transformed into the semi-infinite strip $\xi \geqslant 0, 0 \leqslant \eta \leqslant \pi$. The plate then transforms into $\xi = 0$ with its upper edge at $\eta = \frac{1}{2}\pi$. The upper half of the (ξ, η)-plane contains the upstream region with the centre of the plate at $\eta = \pi$, while the lower half of the (ξ, η)-plane contains the downstream region with the centre of the plate at $\eta = 0$. After all quantities have been made dimensionless, (1)–(3) becomes

$$\frac{\partial u}{\partial t} = -\frac{1}{\phi}\frac{\partial p}{\partial \xi} + \alpha(\xi, \eta), \tag{6}$$

$$\frac{\partial v}{\partial t} = -\frac{1}{\phi}\frac{\partial p}{\partial \eta} + \beta(\xi, \eta), \tag{7}$$

$$\frac{\partial u}{\partial \xi} + \frac{\partial v}{\partial \eta} + \frac{1}{2\phi^2}(u \sinh 2\xi - v \sin 2\eta) = 0, \tag{8}$$

where

$$\left.\begin{aligned}
\phi(\xi, \eta) &= (\cos^2 \eta + \sinh^2 \xi)^{\frac{1}{2}}, \\
\alpha(\xi, \eta) &= -\frac{1}{\phi}\left[\frac{\partial u^2}{\partial \xi} + \frac{\partial (uv)}{\partial \eta}\right] - \frac{1}{2\phi^3}(u^2 \sinh 2\xi - 2uv \sin 2\eta - v^2 \sinh 2\xi) \\
&\quad + \frac{2}{R}\left\{\frac{1}{\phi^2}\left[\frac{\partial^2 u}{\partial \xi^2} + \frac{\partial^2 u}{\partial \eta^2}\right] - \frac{1}{\phi^4}\left[\frac{\partial v}{\partial \xi}\sin 2\eta + \frac{\partial v}{\partial \eta}\sinh 2\xi\right]\right. \\
&\quad \left. + \frac{u}{2\phi^4}(\cos 2\eta - \cosh 2\xi)\right\}, \\
\beta(\xi, \eta) &= -\frac{1}{\phi}\left[\frac{\partial (uv)}{\partial \xi} + \frac{\partial v^2}{\partial \eta}\right] - \frac{1}{2\phi^3}(u^2 \sin 2\eta + 2uv \sinh 2\xi - v^2 \sin 2\eta) \\
&\quad + \frac{2}{R}\left\{\frac{1}{\phi^2}\left[\frac{\partial^2 v}{\partial \xi^2} + \frac{\partial^2 v}{\partial \eta^2}\right] + \frac{1}{\phi^4}\left[\frac{\partial u}{\partial \xi}\sin 2\eta + \frac{\partial u}{\partial \eta}\sinh 2\xi\right]\right. \\
&\quad \left. + \frac{v}{2\phi^4}(\cos 2\eta - \cosh 2\xi)\right\},
\end{aligned}\right\} \tag{9}$$

(u, v) are now the velocity components relative to the (ξ, η)-coordinates and $R = 2Ul/\nu$ is the Reynolds number. The boundary conditions for u and v are now

$$\left.\begin{aligned}
u = v &= 0 \quad \text{on } \xi = 0, \\
v &= 0 \quad \text{on } \eta = 0, \pi, \\
u \to \frac{\cosh \xi \cos \eta}{\phi}, &\quad v \to -\frac{\sinh \xi \sin \eta}{\phi} \quad \text{as } \xi \to \infty.
\end{aligned}\right\} \tag{10}$$

It should be noted that the function $\phi(\xi, \eta)$ is very small near to the top of the plate, and so $\alpha(\xi, \eta)$, $\beta(\xi, \eta)$ are very large in this region. Hence (6) and (7) are not readily amenable to numerical computation: indeed, preliminary numerical experiments confirmed this opinion. It was therefore decided to replace (6) and (7) by equations of the form

$$\frac{\partial u}{\partial t} = \phi^k\left\{-\frac{1}{\phi}\frac{\partial p}{\partial \xi} + \alpha(\xi, \eta)\right\}, \tag{11}$$

$$\frac{\partial v}{\partial t} = \phi^k\left\{-\frac{1}{\phi}\frac{\partial p}{\partial \eta} + \beta(\xi, \eta)\right\}, \tag{12}$$

where k is some suitable constant. Clearly (11) and (12) have the same steady-state solutions as (6) and (7), although the intermediate time-dependent solutions will of course be distorted. Noting that $\phi(\xi, \eta) \to \infty$ as $\xi \to \infty$ it was considered that taking $k = 2$ should ease the computational difficulties near the top of the plate without introducing others at large distance and this, in fact, proved to be the case.

Thus equations (11) and (12) were solved in conjunction with (8) and (10) in the manner described below.

3. Numerical analysis

Let u^n, v^n denote the velocity at time $t = n\,\delta t$ and define functions $\bar{u}(\xi, \eta)$, $\bar{v}(\xi, \eta)$ such that

$$\bar{u} = u^{n+1} + \delta t\, \phi \frac{\partial p}{\partial \xi}, \tag{13}$$

$$\bar{v} = v^{n+1} + \delta t\, \phi \frac{\partial p}{\partial \eta}. \tag{14}$$

Then

$$\frac{\partial u}{\partial t} = \frac{u^{n+1} - u^n}{\delta t} = \frac{\bar{u} - u^n}{\delta t} - \phi \frac{\partial p}{\partial \xi}, \tag{15}$$

$$\frac{\partial v}{\partial t} = \frac{v^{n+1} - v^n}{\delta t} = \frac{\bar{v} - v^n}{\delta t} - \phi \frac{\partial p}{\partial \eta}. \tag{16}$$

Substituting (15) and (16) into (11) and (12) with $k = 2$, the pressure terms are eliminated, giving

$$\bar{u} = u^n + \alpha \phi^2\, \delta t, \tag{17}$$

$$\bar{v} = v^n + \beta \phi^2\, \delta t. \tag{18}$$

Using (13) and (14) to eliminate u and v from (8) produces an equation for the pressure distribution which may be written in the form

$$\frac{\partial}{\partial \xi}\left[\phi^2 \frac{\partial p}{\partial \xi}\right] + \frac{\partial}{\partial \eta}\left[\phi^2 \frac{\partial p}{\partial \eta}\right] = \frac{1}{\delta t}\left[\frac{\partial}{\partial \xi}(\phi \bar{u}) + \frac{\partial}{\partial \eta}(\phi \bar{v})\right]. \tag{19}$$

(It will be shown later that boundary conditions for p are not required.)

Briefly, the procedure adopted for solving the problem is as follows. Assuming that u and v are known at time $t = n\,\delta t$, solutions for $\bar{u}$ and $\bar{v}$ are obtained from (17) and (18). These are then substituted into the right-hand side of (19), which is then solved iteratively for p. To complete the cycle, values of u and v at time $t = (n+1)\,\delta t$ are obtained from (13) and (14). Thus, starting from suitable initial approximations to u and v at time $t = 0$, the above procedure is repeated until steady-state solutions are obtained.

In order to put the above procedure into practice, the region of integration $0 \leqslant \eta \leqslant \pi, 0 \leqslant \xi \leqslant \xi_\infty$ is covered by a square mesh of side h and central finite-difference approximations to the differential equations employed in the manner of Harlow & Welch (1965). Thus the pressure p is defined at the centre of each cell, while the quantities u, $\bar{u}$, v and $\bar{v}$ are defined at the sides of each cell, as shown in figure 2. Here it is only necessary to give the finite-difference approximation to (19), which, in general, may be written (see figure 2)

$$\phi_A^2 p_1 + \phi_B^2 p_2 + \phi_C^2 p_3 + \phi_D^2 p_4 - (\phi_A^2 + \phi_B^2 + \phi_C^2 + \phi_D^2)\, p_0 = \frac{h}{\delta t}[(\phi \bar{u})_A - (\phi \bar{u})_C + (\phi \bar{v})_B - (\phi \bar{v})_D]. \tag{20}$$

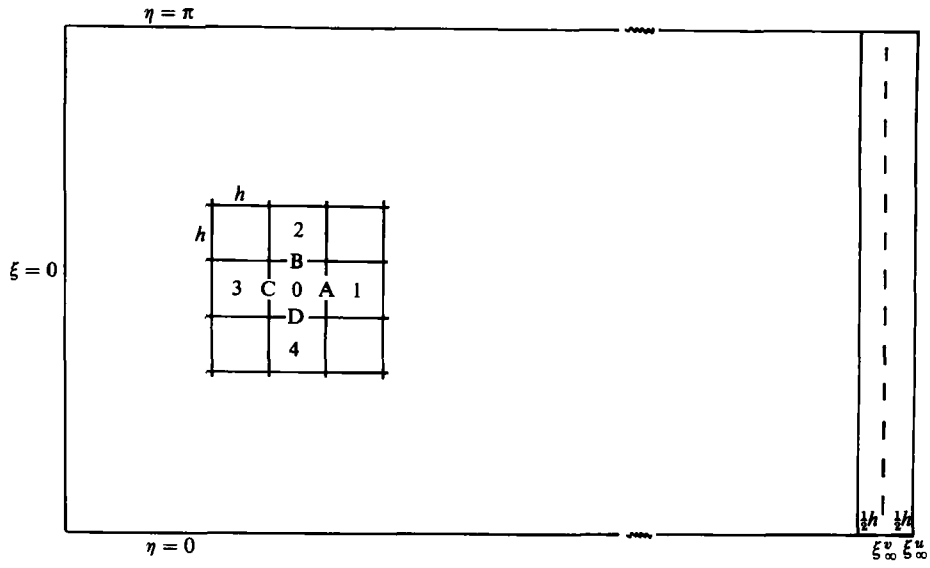

FIGURE 2. The grid structure (p is defined at the points 0, 1, 2, 3, 4; u, $\bar{u}$ at A and C; v, $\bar{v}$ at B and D).

When p_0 is adjacent to a boundary (20) is modified as follows. Next to $\xi = 0$, p_3 and $\bar{u}_C$ are unknown. However, applying (13) on $\xi = 0$ gives

$$\bar{u}_C = \frac{\delta t}{h}\phi_C(p_0 - p_3),$$

from which

$$\phi_C^2 p_3 = \phi_C^2 p_0 - \frac{h}{\delta t}(\phi\bar{u})_C,$$

and substituting in (20) leads to

$$\phi_A^2 p_1 + \phi_B^2 p_2 + \phi_D^2 p_4 - (\phi_A^2 + \phi_B^2 + \phi_D^2) p_0 = \frac{h}{\delta t}[(\phi\bar{u})_A + (\phi\bar{v})_B - (\phi\bar{v})_D].$$

Similarly, when p_0 is next to the outer boundary $\xi = \xi_\infty^u$, p_1 and $\bar{u}_A$ are unknown, but, by applying (13) on $\xi = \xi_\infty^u$, we can reduce (20) to the form

$$\phi_A^2 p_2 + \phi_C^2 p_3 + \phi_D^2 p_4 - (\phi_B^2 + \phi_C^2 + \phi_D^2) p_0 = \frac{h}{\delta t}[(\phi u) - (\phi\bar{u})_C + (\phi\bar{v})_B - (\phi\bar{v})_D],$$

where the term ϕu is evaluated on the boundary $\xi = \xi_\infty^u$ (see figure 2). Thus, noting also that

$$p_4 = p_0, \quad \bar{v}_D = 0 \quad \text{when } p_0 \text{ is adjacent to } \eta = 0,$$
$$p_2 = p_0, \quad \bar{v}_B = 0 \quad \text{when } p_0 \text{ is adjacent to } \eta = \pi,$$

it can be seen that the only boundary conditions required are those for u and v. However, as mentioned in Roache (1976), it is convenient (but not essential) to restrict one nodal value of p at large distance upstream to zero, and this was done in the present calculations.

Various methods are available to implement the conditions given in (10). After some numerical investigation, it was decided to use the free-stream conditions

explicitly on the upstream boundary, but on the downstream boundary to adopt the approach of Slotta *et al.* (1969). With reference to figure 2, values of v on $\xi = \xi^v_\infty$ are evaluated from known internal values, while those for u on $\xi = \xi^u_\infty$ are obtained from the equation of continuity as follows. Differentiating the second of (10) and applying the resulting equation on $\xi = \xi^u_\infty$ leads to the approximation

$$v(\xi^v_\infty, \eta) \sim v(\xi^v_\infty - h, \eta) - h \sin\eta \cos^2\eta \left[\frac{\cosh\xi}{\phi^3}\right]_{\xi = \xi^u_\infty}, \tag{21}$$

and applying (8) to each cell with centre on the line $\xi = \xi^v_\infty$ yields

$$u(\xi^u_\infty, \eta) \sim \frac{(1-\lambda)\,u(\xi^u_\infty - h, \eta) - (1-\mu)\,v(\xi^v_\infty, \eta - \tfrac{1}{2}h) + (1+\mu)\,v(\xi^v_\infty, \eta + \tfrac{1}{2}h)}{1+\lambda}, \tag{22}$$

where

$$\lambda(\eta) = \frac{h}{4}\left[\frac{\sinh 2\xi}{\phi^2}\right]_{\xi = \xi^v_\infty},$$

$$\mu(\eta) = \frac{h}{4}\left[\frac{\sin 2\eta}{\phi^2}\right]_{\xi = \xi^v_\infty}.$$

4. Results and discussion

Solutions were obtained for Reynolds numbers $R = 0.1$, 0.2, 0.5, 1, 5, 10 and 20. In each case the computations were started from the free-stream solution (i.e. the values of u and v were set equal to their free-stream value everywhere except on the plate itself) and terminated when

$$\sum_{i,j}\left|1 - \frac{u^n_{i,j}}{u^{n+1}_{i,j}}\right|, \quad \sum_{i,j}\left|1 - \frac{v^n_{i,j}}{v^{n+1}_{i,j}}\right| \leqslant \epsilon,$$

where the summations include all nodal values of u and v respectively, and ϵ is some preassigned exit tolerance. Initially, ϵ was set equal to 10^{-4} and then reduced to 10^{-5}. Examination of the respective solutions for u, v and p showed little or no change in the fifth significant figures, and so it was assumed that the steady-state solution had been attained by this stage and that further reduction of ϵ was unnecessary. The solutions appeared to converge satisfactorily to their final values with the given assumption for the initial flow. Of course, once a final steady-state solution had been obtained for one Reynolds number, it could be used as a starting approximation for the next. This alternative assumption for the initial flow was in fact investigated for one value of R, but the rate of convergence of the numerical procedure was not improved.

Details of the main computational parameters are given in table 1. For all Reynolds numbers solutions were obtained with $h = \frac{1}{30}\pi$. In order to assess the effect of grid size, an additional solution was computed for $R = 10$ with $h = \frac{1}{60}\pi$. The latter calculations proved to be expensive in computer time, and, in view of the excellent agreement (see below) between the solutions on the different grids at this Reynolds number, no attempt was made to calculate fine-mesh solutions for other values of R.

The choice of δt was governed by the question of stability and determined by numerical experiment. As table 1 shows, the lower Reynolds number required the smallest values of δt. Values of T, the total time taken to attain the converged steady-state solution, are also recorded in this table.

The final column of table 1 indicates the maximum distance at which the outer

R	h	δt	T	ξ_∞^u
0.1	$\frac{1}{30}\pi$	0.0001	0.5314	$\frac{5}{3}\pi$
0.2	$\frac{1}{30}\pi$	0.0002	0.9986	$\frac{5}{3}\pi$
0.5	$\frac{1}{30}\pi$	0.0005	2.0385	$\frac{5}{3}\pi$
1	$\frac{1}{30}\pi$	0.001	3.2780	$\frac{5}{3}\pi$
5	$\frac{1}{30}\pi$	0.001	12.272	$\frac{3}{2}\pi$
10	$\frac{1}{30}\pi$	0.001	15.527	$\frac{4}{3}\pi$
10*	$\frac{1}{60}\pi$	0.0005	9.4805	$\frac{7}{6}\pi$
20	$\frac{1}{30}\pi$	0.001	18.012	$\frac{7}{6}\pi$

TABLE 1. Computational parameters (see text)

boundary conditions were applied. It is well known that, when dealing with fluid flows past bluff bodies, the position of the outer boundary has to be chosen with care, as the solution in the neighbourhood of the bluff body can be adversely affected by both the type and the proximity of the outer boundary conditions. This problem has been studied in detail in the case of flow past a sphere by Hudson (1974). The main difficulty is in the calculation of the downstream flow, and it appears that the problem is less serious when the conditions on the downstream boundary are computed from the upstream solution. This is an important feature of the present calculations. Nevertheless, any outer boundary conditions should ideally be initially placed at some arbitrary point ξ_∞, and then the magnitude of ξ_∞ increased until there is no significant change in the solution near to the solid body. In practice, however, numerical instability can impose an upper bound ξ_∞^* on the magnitude of ξ_∞, and this bound usually reduces as the Reynolds number increases. This was found to be the case in the current work, and, with the exception of the fine-mesh calculations for $R = 10$, the values of ξ_∞^u given in table 1 coincide with the corresponding values of ξ_∞^* for $R \geqslant 5$. For this reason, no attempt was made to extend the present calculations beyond $R = 20$.

In order to check that the maximum values of ξ_∞ used were satisfactory, the following tests were carried out. At $R = 5$ solutions were obtained with (i) $\xi_\infty = \frac{4}{3}\pi$ and (ii) $\xi_\infty = \frac{3}{2}\pi$. It was noted that the dimensionless eddy length x_l (obtained by dividing the actual eddy length by the half-plate length l) change from 1.35 to 1.34. At $R = 10$ solutions were obtained with (i) $\xi_\infty = \frac{7}{6}\pi$ and (ii) $\xi_\infty = \frac{4}{3}\pi$: the corresponding values of x_l were found to be 2.41 and 2.40 respectively. For $R = 20$ solutions were obtained with (i) $\xi_\infty = \pi$ and (ii) $\xi_\infty = \frac{7}{6}\pi$. This is equivalent to increasing the dimensionless distance x/l from the relatively low value of 11.5 to 19.5, and in this case x_l changed from 4.43 to 4.65. These experiments suggest that the values of ξ_∞ employed were sufficiently large and also that the boundary conditions given in (21) and (22) are not unduly sensitive to the effects of boundary distance.

At this point it is convenient to mention the fine-mesh solution for $R = 10$, which produced a value of $x_l = 2.43$ with $\xi_\infty = \frac{7}{6}\pi$. Comparing this with the value $x_l = 2.41$ given above for the coarse mesh with the same boundary distance indicates the adequacy of the $h = \frac{1}{30}\pi$ grid size at this Reynolds number, and suggests that the results obtained using this grid for $R = 20$ are at least of reasonable accuracy. Further evidence for this view is available in table 2, where the results for the two different grid sizes at $R = 10$ indicate only very small changes in other properties of the flow in the wake with the change in grid size.

R	x_l	y_w	x_c	y_c	ψ_c
0.1	0.11	1	0.008	0.92	-0.77×10^{-5}
0.2	0.13	1	0.032	0.65	-0.97×10^{-5}
0.5	0.27	1	0.10	0.57	-0.11×10^{-3}
1	0.45	1	0.20	0.52	-0.48×10^{-3}
5	1.34	1	0.57	0.56	-0.11×10^{-1}
10	2.40	1.12	0.88	0.64	-0.36×10^{-1}
10*	2.43	1.13	0.89	0.65	-0.38×10^{-1}
20	4.65	1.35	1.44	0.76	-0.95×10^{-1}

TABLE 2. Wake dimensions and details of the vortex centre (see text)

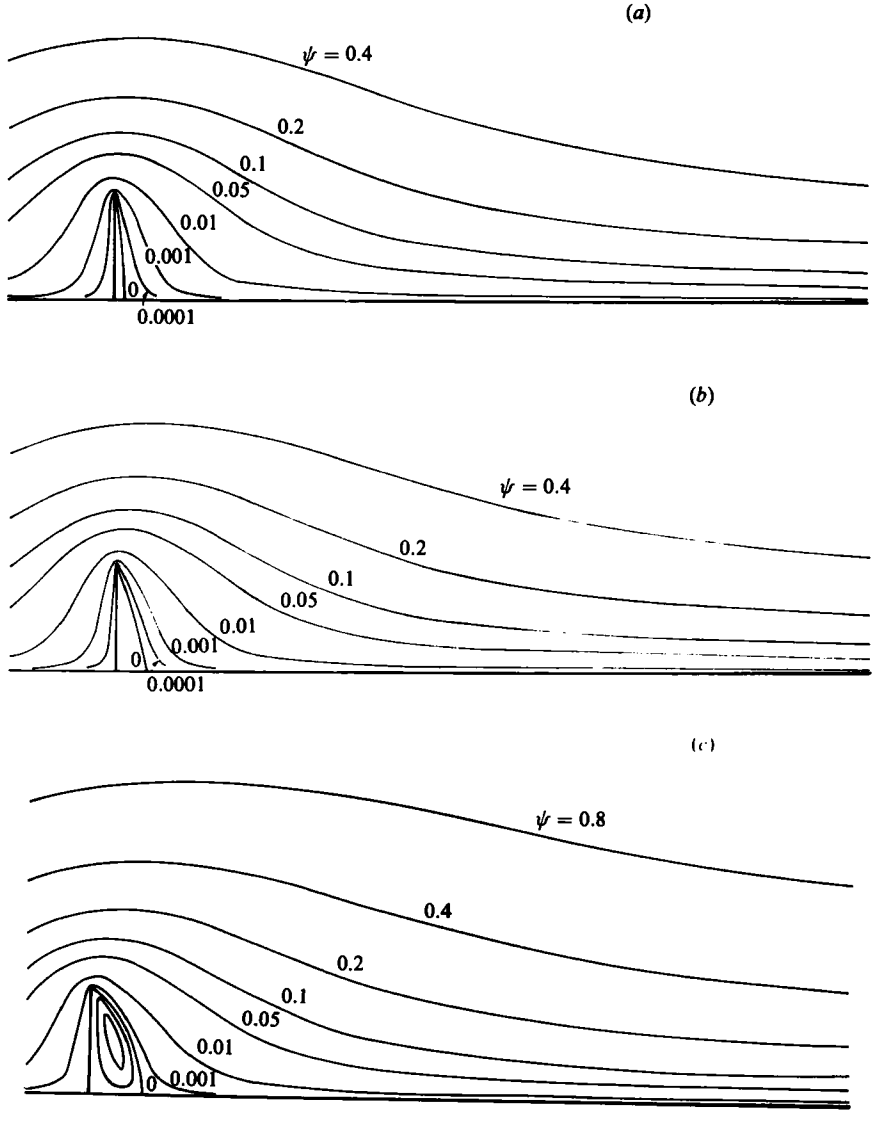

FIGURE 3 (*a–c*). For caption see next page.

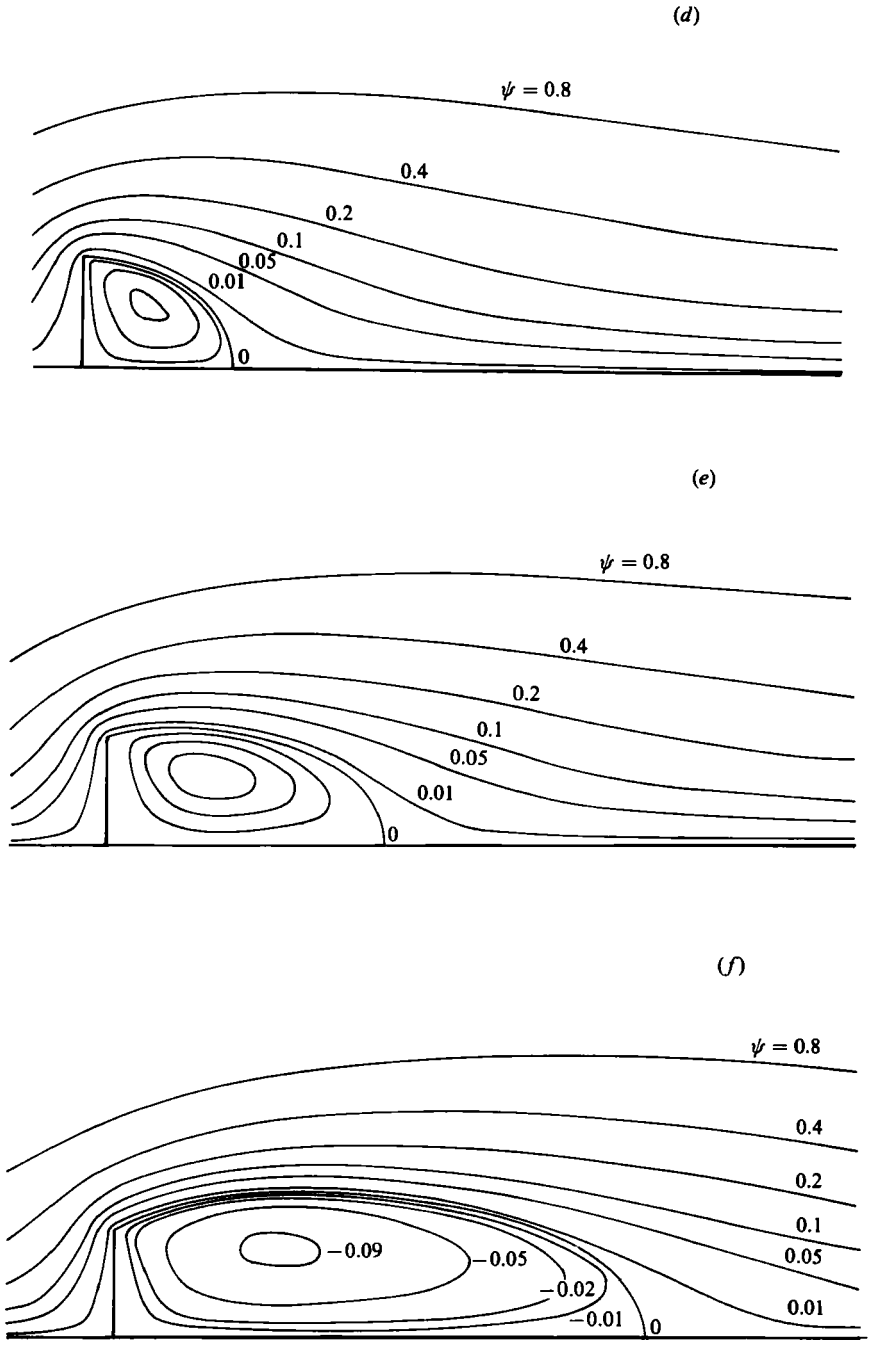

FIGURE 3. Streamlines for (*a*) $R = 0.1$; (*b*) 0.5; (*c*) 1 (enclosed streamlines, starting from the centre, are $\psi = -0.0004, -0.0002$); (*d*) 5 (enclosed streamlines are $\psi = -0.01, -0.005, -0.002$); (*e*) 10 (enclosed streamlines are $\psi = -0.03, -0.02, \psi = -0.01$); (*f*) 20 (enclosed streamlines are $\psi = -0.09, -0.05, -0.02, -0.01$).

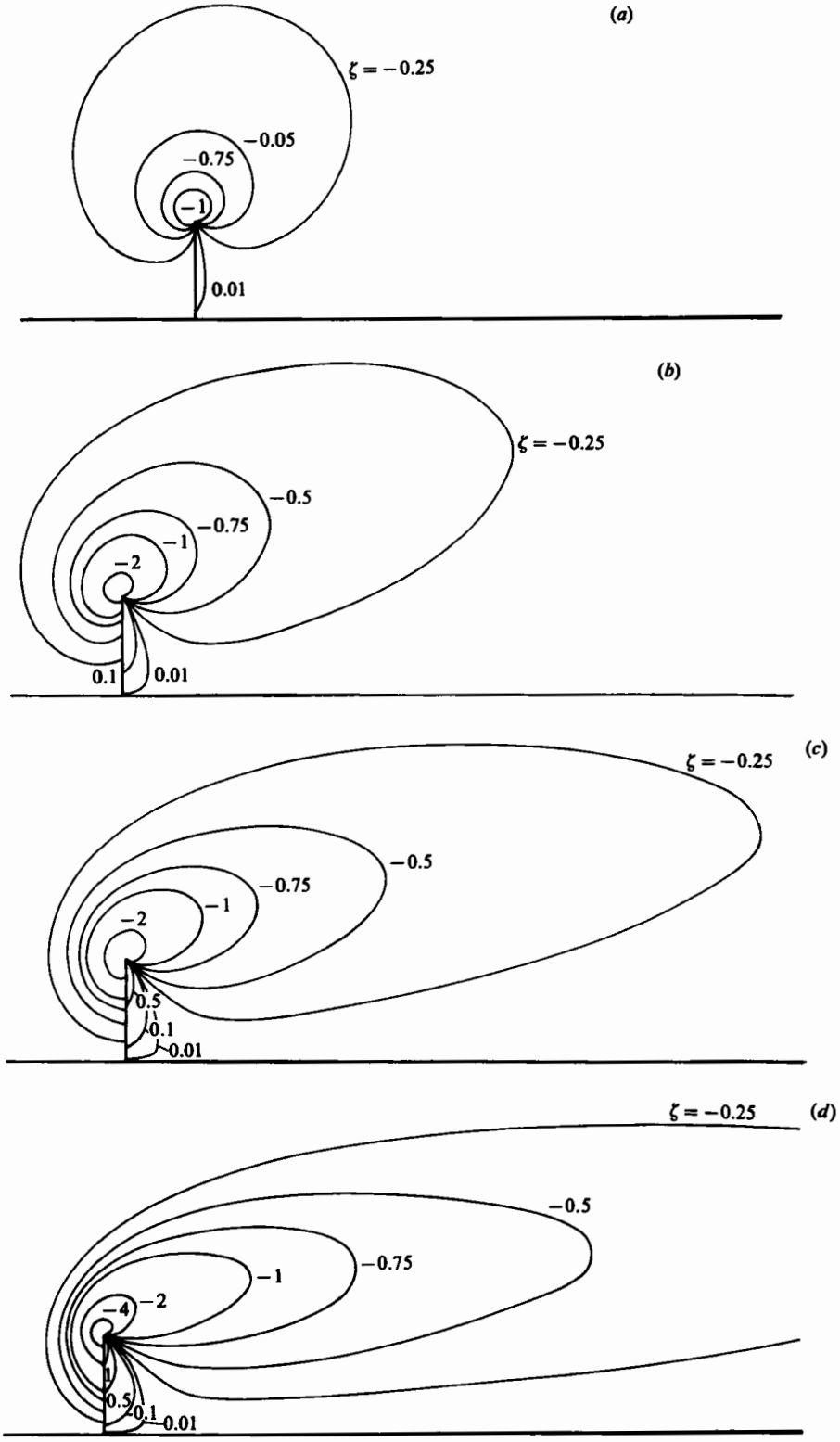

FIGURE 4. Equivorticity lines for (*a*) $R = 1$; (*b*) 5; (*c*) 10; (*d*) 20.

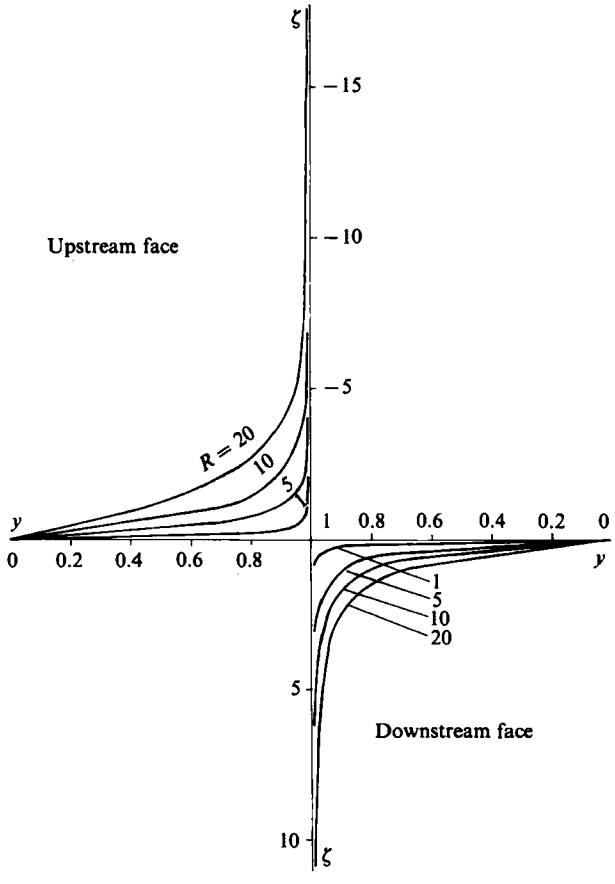

FIGURE 5. Vorticity distribution on the surface of the plate.

From the steady-state solutions for u and v, the stream function ψ and the vorticity ζ were calculated using the formulae

$$\psi(\xi, \eta_0) = -\int_0^{\xi} \phi(z, \eta_0)\, v(z, \eta_0)\, \mathrm{d}z, \tag{23}$$

$$\zeta(\xi, \eta) = \frac{1}{\phi}\left\{\frac{\partial v}{\partial \xi} - \frac{\partial u}{\partial \eta}\right\} + \frac{1}{2\phi^3}\{v \sinh 2\xi + u \sin 2\eta\}. \tag{24}$$

Some checks on the calculation of the stream function were made by calculating ψ from the velocity component u using an equation corresponding to (23). This was found to yield streamlines that were essentially the same as those calculated from (23).

Streamlines and equivorticity lines are presented in figures 3 and 4 respectively, while the vorticity on the surface of the plate is shown in figure 5. The present calculations exhibit clearly the presence of an eddy behind the plate even at the smallest Reynolds number considered ($R = 0.1$), and this is in accordance with the predictions of Imai (1957) and Miyagi (1978) from Oseen theory.

Eddy dimensions are given in table 2. The dimensionless eddy lengths x_l are plotted against the Reynolds number for $R \geqslant 1$ in figure 6, where they are compared with

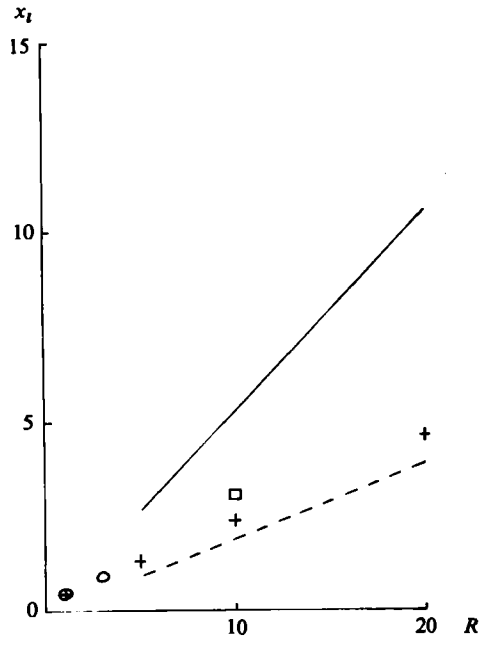

FIGURE 6. Eddy length against Reynolds number; comparison with previous results: ——, Smith; --- Acrivos *et al.*; ○, Taneda; □, Prandtl & Tietjens; +, present results.

the results of other workers. The present results appear to be in excellent agreement with the experimental work of Taneda (taken from Miyagi 1978) and in reasonable agreement with that of Prandtl & Tietjens (1934) at $R = 10$. This latter experimental point is taken from Batchelor (1967, plate 4) and could be subject to some slight error of interpretation. The present calculated results are much lower than the theoretical estimates of Smith (1979). However, it is perhaps relevant to point out that, in the case of the circular cylinder, the eddy lengths estimated by Smith are also substantially higher than other computed results. The final comparison made in figure 6 is with the experimental results of Acrivos *et al.* (1968). From their table 1 (p. 29) we find the empirical formula

$$x_l = 0.194R$$

in the present notation, and, although this is only strictly applicable at rather higher Reynolds numbers than those of the present investigation, the agreement with the present work at lower R is very favourable. Moreover, the experiments were carried out with a finite blockage ratio, which always shortens the wake marginally, so in reality the agreement could be even better than that suggested by figure 6. Finally, on the subject of eddy lengths, it should be noted that the estimates of x_l for low R obtained by Miyagi (1978) from Oseen theory are significantly higher than those of both the present investigation and the experimental results of Taneda.

With regard to the eddy half-width y_w, the present results indicate that y_w remains at approximately unity at least as far as $R = 5$. However, at $R = 20$, y_w has increased to 1.35. Although the Reynolds numbers here are rather small, it could be noted in passing that this latter result tends to favour the theory of Smith (i.e. $y_w \propto R^{\frac{1}{2}}$) rather than the model proposed by Acrivos *et al.* (i.e. $y_w = O(1)$), although in our case the proportionality constant is some 20 % lower than the value 0.385 of Smith. It is again

encouraging to note reasonable agreement with the experimental results of Prandtl & Tietjens for y_w.

Table 2 also gives the coordinates (x_c, y_c) of the vortex centre and the magnitude of the stream function ψ_c at this point. At $R = 0.1$ the vortex centre is very close to the top of the plate. However, as R increases from 0.1 to about 1, it moves away from the plate but nearer to the axis of symmetry. Between $R = 1$ and $R = 20$ the vortex centre continues to leave the plate, but also moves away from the axis of symmetry. Acrivos *et al.* observed experimentally that $x_c/x_l \approx 0.33$ for $R > 30$, and it is interesting to note that our results at $R = 20$ give 0.31 for this ratio. Furthermore, the experimental work also suggested that $y_c/y_w \approx 0.6$ for $R > 30$, while our results at $R = 20$ give 0.56 for this value. Although the values of y_w observed by Acrivos *et al.* will probably have been affected by the containing walls (see Smith 1979), the estimates of y_c will also have been affected in a similar manner. Thus the satisfactory agreement of the ratio of these two quantities with our own result could still be a realistic comparison. The values of ψ_c in table 2 are given primarily for reference in possible future work.

Finally, one other comparison may be made at this stage with the observations of Acrivos *et al.* They observed that the backflow velocity $-u/U$ along the returning stagnation streamline was independent of R (for large R) and nearly constant (≈ 0.17) over a large portion of the wake. The present calculations show that this velocity lies between 0.16 and 0.18 over approximately one-third of the recirculating wake for $R = 20$, which is of the same order of magnitude as the experimental result.

5. Conclusions

The research described in this paper appears to be the first attempt to obtain numerical solutions of the Navier–Stokes equations for the case of the normal flat plate. Reasonable care has been taken to ensure that the eddy dimensions have not been adversely affected either by the proximity of the outer boundary or by the premature termination of the iterative procedure. Indeed, with regard to the latter, one of the solutions was inadvertently iterated for almost twice the time required by the rather severe convergence test, but this had no effect whatsoever on the eddy dimensions. The general agreement of many features of the present results with those of experiments is satisfactory. The agreement of the calculated results for the two grid sizes $h = \frac{1}{30}\pi$ and $\frac{1}{60}\pi$ at $R = 10$ is satisfactory enough to suggest that the calculations are accurate enough within the range of Reynolds numbers considered.

It will be apparent that the method of solution outlined above has a number of flexible features which invite further experimentation and a few other possibilities have in fact been explored. For example, one version of the computer program was based on a slightly different analysis, which used $k = 1$ in (11) and (12), while another version of the program applied the free-stream conditions on the outer boundary in place of (21) and (22). Whilst these particular alternatives proved to be generally inferior to the scheme described here, it is appreciated that the scheme finally adopted is not necessarily the most efficient. Nevertheless, the lack of necessity of calculating the vorticity and pressure on the plate is a very positive feature of the method. In a vorticity–stream-function formulation of this problem there would be great difficulties in calculating the vorticity at the edges of the plate.

In conclusion, the authors would like to record their gratitude to Mr D. J. Mullings for general programming assistance and in particular for providing the graph-plotting routines.

REFERENCES

ACRIVOS, A., SNOWDEN, D. D., GROVE, A. S. & PETERSON, E. E. 1965 The steady separated flow past a circular cylinder at large Reynolds numbers. *J. Fluid Mech.* **21**, 737.

ACRIVOS, A., LEAL, L. G., SNOWDEN, D. D. & PAN, F. 1968 Further experiments on steady separated flows past bluff objects. *J. Fluid Mech.* **34**, 25.

BATCHELOR, G. K. 1967 *An Introduction to Fluid Dynamics*. Cambridge University Press.

BELOTSERKOVSKII, O. M., GUSHCHIN, V. A. & SHCHENNIKOV, V. V. 1975 Use of the splitting method to solve problems of the dynamics of a viscous fluid. *USSR Comp. Maths & Math. Phys.* **15**, 190.

DENNIS, S. C. R. & HUDSON, J. D. 1980 Further accurate representations of partial differential equations by finite-difference methods. *J. Inst. Maths Applics* **26**, 369.

HARLOW, F. H. & WELCH, J. E. 1965 Numerical calculation of time-dependent viscous incompressible flow of fluid with free surface. *Phys. Fluids* **8**, 2182.

HUDSON, J. D. 1974 Problems relating to the steady motion of a viscous incompressible fluid past a sphere. Ph.D. Thesis, University of Sheffield.

IMAI, I. 1957 *Univ. Maryland Inst. Fluid Dyn. Appl. Maths Tech. Note* BN-104.

MIYAGI, T. 1968 Numerical study of Oseen flow past a perpendicular flat plate. *J. Phys. Soc. Japan* **24**, 204.

MIYAGI, T. 1978 Standing vortex pair behind a flat plate normal to uniform flow of a viscous fluid. *J. Phys. Soc. Japan* **45**, 175.

PRANDTL, L. & TIETJENS, O. G. 1934 *Applied Hydro- and Aeromechanics*. McGraw-Hill.

ROACHE, P. J. 1972 *Computational Fluid Dynamics*. Hermosa.

SLOTTA, L. S., ELWIN, E. H., MERCIER, H. T. & TERRY, M. D. 1969 Stratified reservoir currents. *Bull.* 44, *Engng Expt Station, Oregon State Univ.*

SMITH, F. T. 1979 Laminar flow of an incompressible fluid past a bluff body: the separation, reattachment, eddy properties and drag. *J. Fluid Mech.* **92**, 171.

TAMEDA, K. & MIYAGI, T. 1962 Laminar viscous flow past a perpendicular flat plate with special reference to high Reynolds numbers. *J. Phys. Soc. Japan* **17**, 373.

TANEDA, S. 1968 *Rep. Res. Inst. Appl. Mech. Kyushu Univ.* **16**, 155.

TOMOTIKA, A. & AOI, T. 1953 The steady flow of a viscous fluid past an elliptic cylinder and a flat plate at small Reynolds numbers. *Q. J. Mech. Appl. Maths* **6**, 294.